1 **Threshold Atmospheric Electric Fields for Initiating Relativistic Runaway Electron**
2 **Avalanches: Theoretical Estimates and CORSIKA Simulations**

3 Ashot Chilingarian[*], Liza Hovhannisyan, Mary Zazyan

4 A I Alikhanyan national lab (Yerevan Physics Institute), Alikhanyan Brothers 2, Yerevan
5 36, Armenia

6 *corresponding author chili@aragats.am

7 **Abstract**

8 We examine the threshold Atmospheric Electric Field (E_{th}) needed to initiate a runaway
9 avalanche process in Earth's atmosphere. We compare the traditional, thirty-year-old
10 theoretical threshold value with its recently updated value, along with the threshold
11 derived from CORSIKA-simulated avalanches (E_z). The altitude dependence of these
12 threshold values is analyzed, considering changes in air density and their effects on
13 avalanche development. This study is vital for understanding high-energy atmospheric
14 phenomena in both the lower and upper atmosphere, including thunderstorm ground
15 enhancements (TGEs) and gamma glows, as well as for refining AEF models based on
16 particle flux measurements.

17 **Short Summary**

18 Thunderstorms can accelerate particles in the atmosphere, producing bursts of radiation at
19 the ground. We investigated how strong the electric field inside a cloud must be to start
20 such events. Using advanced computer simulations and comparing with measurements
21 from mountain stations, we found that fields must be stronger than earlier theory
22 suggested. Our results improve understanding of storm electricity and its role in natural
23 radiation.

24 **Highlights**

25 • Introduces a refined framework for determining threshold atmospheric electric
26 fields (E_{th}) needed to initiate relativistic runaway electron avalanches (RREAs)
27 and thunderstorm ground enhancements (TGEs).
28 • Compares classical ($E_{th} \approx 2.80 \times n$) and updated ($E_{th} \approx 2.67 \times n$) theoretical
29 thresholds with altitude-dependent thresholds derived from CORSIKA
30 simulations.
31 • Demonstrates that realistic avalanche development requires fields 15–22%
32 stronger than theoretical values, depending on altitude and air density.
33 • Provides a reproducible simulation methodology for integrating experimental
34 particle flux measurements into atmospheric electricity models across multiple
35 research stations.

Introduction

Free electrons are abundant in the troposphere. The altitude where their density reaches its highest point—called the Regener–Pfotzer maximum—depends on various factors, including the geomagnetic cutoff rigidity (Rc), the type of particles being measured, and the phase and strength of the solar cycle. Recent observations, supported by PARMA4.0 calculations (Sato, 2016), show that at middle to low latitudes (Rc = 3–8 GV), the highest flux of charged particles occurs at altitudes around 12–14 km (see Fig. 4 in Ambrozova et al., 2023).

Atmospheric electric fields (AEFs) generated by thunderstorms transfer energy to free electrons, accelerate them, and, under certain conditions, induce electron-photon avalanches. In 1992, Gurevich, Milikh, and Roussel-Dupré identified the conditions necessary for extensive multiplication of electrons from each energetic seed electron injected into a strong AEF region (Gurevich et al., 1992). This process is known as the Relativistic Runaway Electron Avalanche (RREA; Babich et al., 2001; Alexeenko et al., 2002). A numerical approach for solving the relativistic Boltzmann equation for runaway electron beams (Symbalisty et al., 1998) aids in estimating the threshold AEF (Babich et al., 2001; Dwyer et al., 2003) required to trigger RREA. As demonstrated by GEANT4 and CORSIKA simulations (Chilingarian et al., 2012, 2022), the RREA process is a threshold phenomenon, with avalanches initiating when the atmospheric AEF exceeds a certain threshold, which depends on the air density. The AEF must also be sufficiently extended to support the growth of avalanches. At standard temperature and pressure in dry air at sea level, $E_{th} \approx 2.80 * n$ kV/cm, where air density n is relative to the International Standard Atmosphere (ISA) sea-level value (see the recent update of the threshold energy $E_{th} \approx 2.67 * n$ kV/cm in Dwyer and Rassoul, 2024).

This threshold field is slightly higher than the breakeven field, which corresponds to the electron energy at which minimum ionization occurs. If electrons traveled exactly along AEF lines, it would define the threshold for runaway electron propagation and the start of avalanche formation. However, the paths of electrons deviate due to Coulomb scattering with atomic nuclei and Møller scattering with atomic electrons, causing deviations from the near-vertical AEF. Additionally, secondary electrons produced by Møller scattering are not generated along the field line; therefore, AEFs 10-20% stronger are required for electrons to run away and trigger an avalanche.

1. Corsika simulations of RREAs reaching on Aragats stations

To understand how avalanches develop in an electrified atmosphere and to compare the new and updated E_{th} with the particle intensity growth, we used the CORSIKA code (Heck et al., 1998), version 7400, which takes into account the effect of AEFs on particle
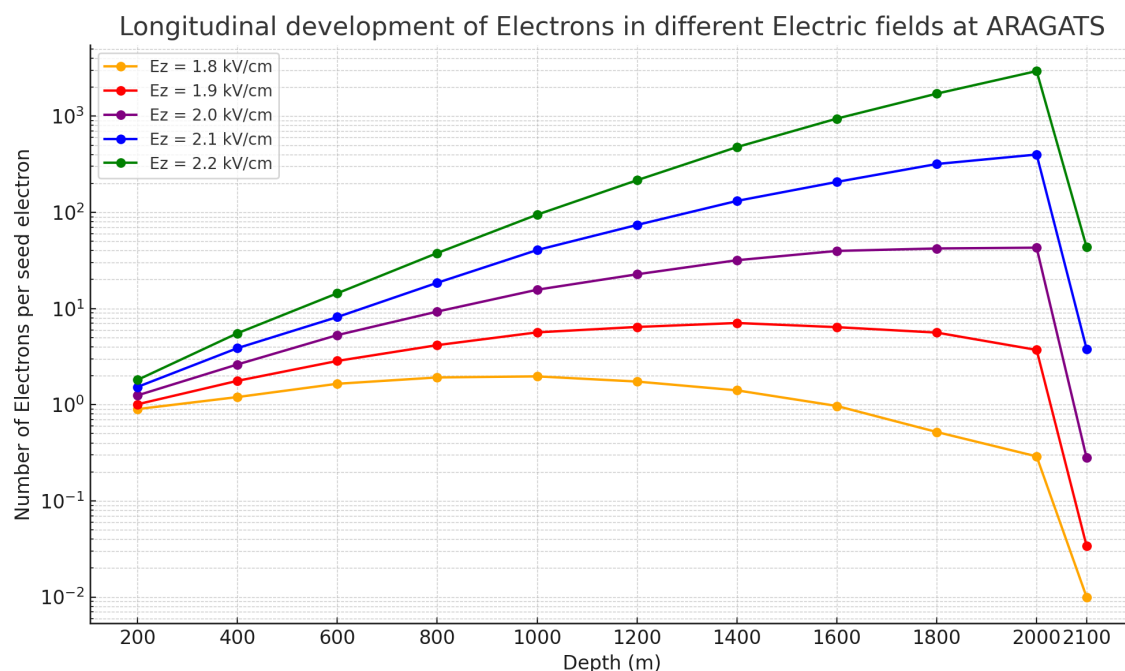
72   transport (Butnik et al., 2010). The growth of RREA definitely increases the cloud's
73   electrical conductivity. Numerous studies (Marshall et al., 1995; Stolzenburg et al., 2007)
74   have indicated that lightning flashes occur after the RREA threshold exceeds 20-30%.
75   RREA simulation codes do not include a lightning initiation mechanism. Therefore, one
76   can artificially raise the AEF strength beyond a realistic value to produce billions of
77   avalanche particles; however, this approach lacks physical justification. As a result, we
78   do not test AEFs stronger than 2.2 kV/m at altitudes of 3-6 km. The RREA simulation
79   was performed for vertical seed electrons with a uniform AEF that exceeded the E_{th} by a
80   few tens of percent. An introduced fixed uniform AEF shifts the surplus to E_{th} at different
81   heights by different percent, corresponding to air density. The seed electron energy
82   spectrum was based on the EXPACS WEB calculator (Sato, 2018), following a power
83   law with an index of 1.173 for energies from 1 to 300 MeV. During TGE events on
84   Aragats, the typical distance to the cloud base is estimated to be 25–200 m (see Fig. 17 in
85   Chilingarian et al., 2020); therefore, in our simulations, particle propagation continued in
86   dense air for an additional 25, 50, 100, and 200 meters before detection. The simulations
87   included 1,000 to 10,000 events for AEF strengths from 1.55 to 2.5 kV/cm. Electron and
88   gamma-ray propagation was tracked until their energies dropped to 0.05 MeV. The
89   CORSIKA code models RREA development, calculating the number of electrons and
90   gamma rays at various stages within the AEF, every 200 m.

91   Besides the Aragats and Nor Amberd research stations on the slopes of Mt. Aragats in
92   Armenia, we also conducted simulations for Slovakian and Chinese research stations at
93   Lomnicky Stit and the Tibetan plateau. LHAASO (Large High Altitude Air Shower
94   Observatory) is situated at 4410 meters above sea level. It provides an ideal platform for
95   studying atmospheric particle acceleration due to its thin atmosphere and high likelihood
96   of runaway electron avalanche formation. We present CORSIKA simulation results
97   showing increases in electron and photon fluxes under AEF strengths ranging from 1.55
98   to 1.9 kV/m. The number of electrons and photons was recorded at depths ranging from
99   6510 meters to 4510 meters.
100   Lomnický Štít is located at an altitude of 2630 meters in Slovakia. CORSIKA simulations
101   were performed for various vertical AEFs ranging from 1.9 to 2.3 kV/cm. The number of
102   electrons and photons was recorded at depths ranging from 4734 meters to 2734 meters.
103   Significant increases in flux were observed with stronger fields, confirming the
104   development of robust RREA. Saturation trends in the growth of electrons and photons
105   suggest that the threshold field, Eth, at Lomnický Štít is approximately 2.3 kV/cm. These
106   results support earlier findings from Aragats and Nor Amberd and emphasize the altitude
107   dependence of Eth. Due to the thinner air, at Lhasso, the TGEs occurred at a much lower
108   value of 1.7 kV/m.
109   In Figures 1-4, we display the development of RRE avalanches at different atmospheric
110   depths and for various physically justified strengths of the AEF. The curves are scaled for
111   a single seed electron for easier comparison with experimentally measured intensities.
112   For each lower value of AEF, we observe saturation of the particle flux; the RREA

113 process attenuates before reaching the observation level (see the red and yellow curves in
114 Figs. 1-4).
115

116
117 **Figure 1. Development of the RRE avalanche in the atmosphere. The avalanche**
118 **started at 5400 meters above sea level, which is 2100 meters higher than the Aragats**
119 **station. The number of avalanche particles is calculated every 200 meters. After**
120 **leaving the AEF, the movement of avalanche particles is tracked for an additional**
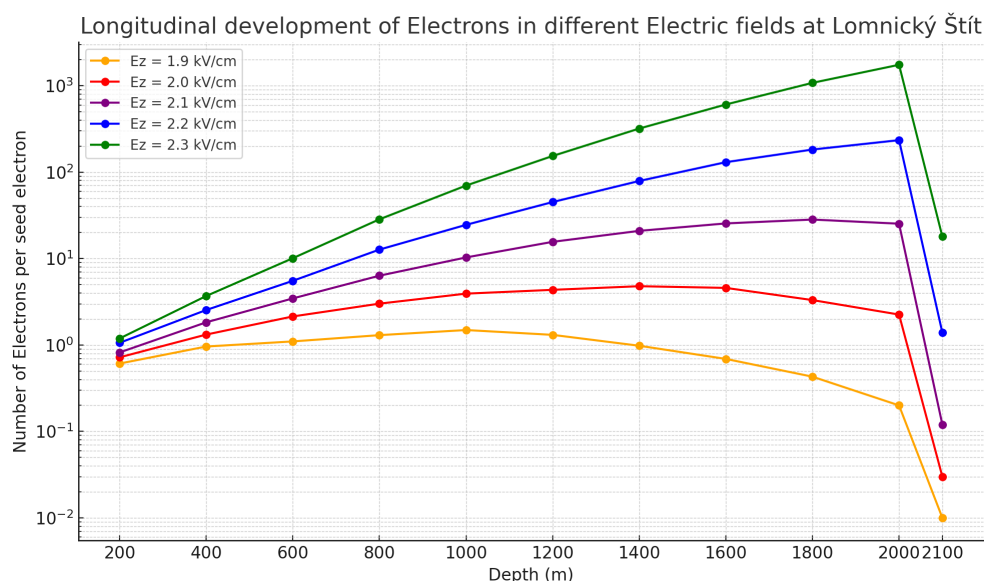121 **100 meters before reaching the station.**

122

Figure 2. Development of the RRE avalanche in the atmosphere. The avalanche started at 4730 meters above sea level, which is 2100 meters higher than the Lomnicky Stit station. The number of avalanche particles is calculated every 200 meters. After leaving the AEF, the movement of avalanche particles is tracked for an additional 100 meters before reaching the station.
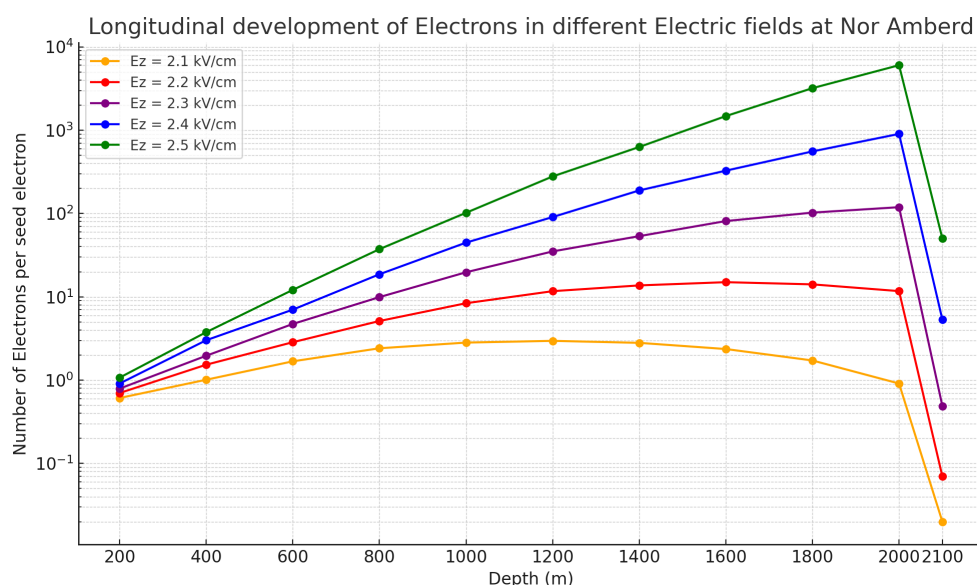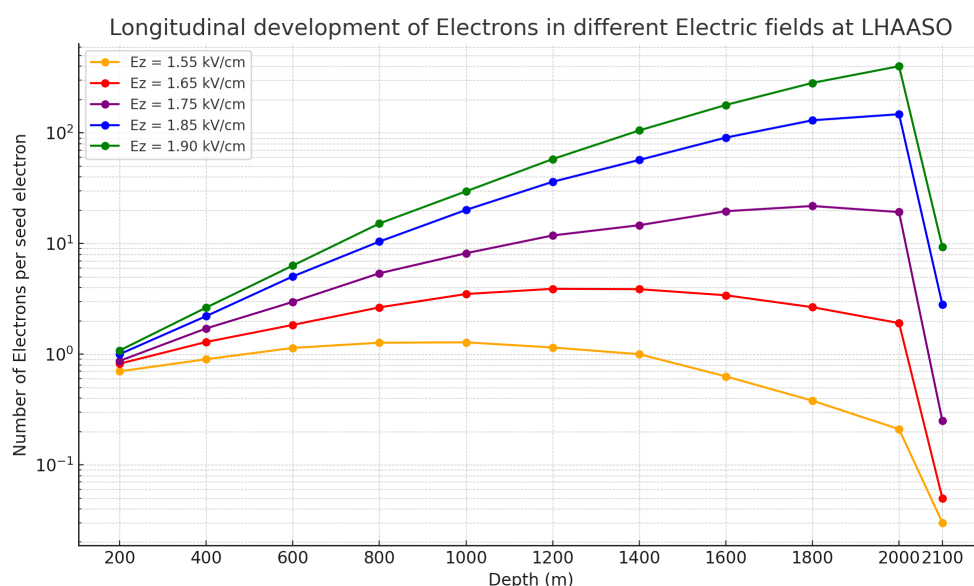
123
124
125
126
127

128

Figure 3. Development of the RRE avalanche in the atmosphere. The avalanche began at 4100 m a.s.l. (0 meters depth), which is 2100 meters above the Nor Amberd station. The number of avalanche particles is calculated every 200 meters. After

129
130
131

132 **exiting the AEF, the propagation of avalanche particles is tracked for an additional**
133 **100 meters before reaching the station.**

134

135

136
137 **Figure 4. Development of the RRE avalanche in the atmosphere. The avalanche**
138 **started at 6510 meters above sea level, which is 2100 meters higher than the**
139 **LHAASO station. The number of avalanche particles is calculated every 200 meters.**
140 **After leaving the AEF, the movement of avalanche particles is tracked for an**
141 **additional 100 meters before reaching the station.**

142
143 We estimate the "simulated" thresholds, E_z values, at the heights at which the amount of
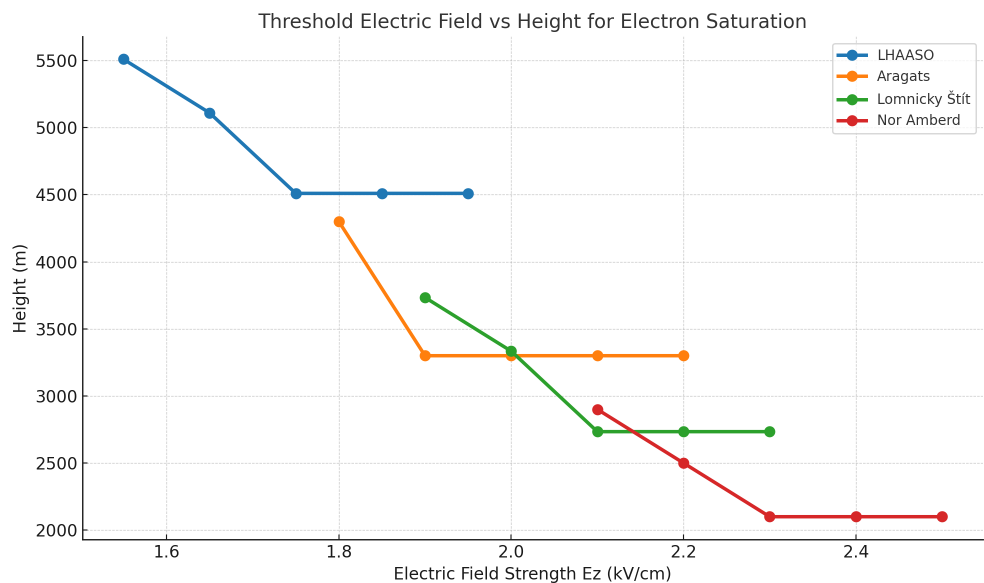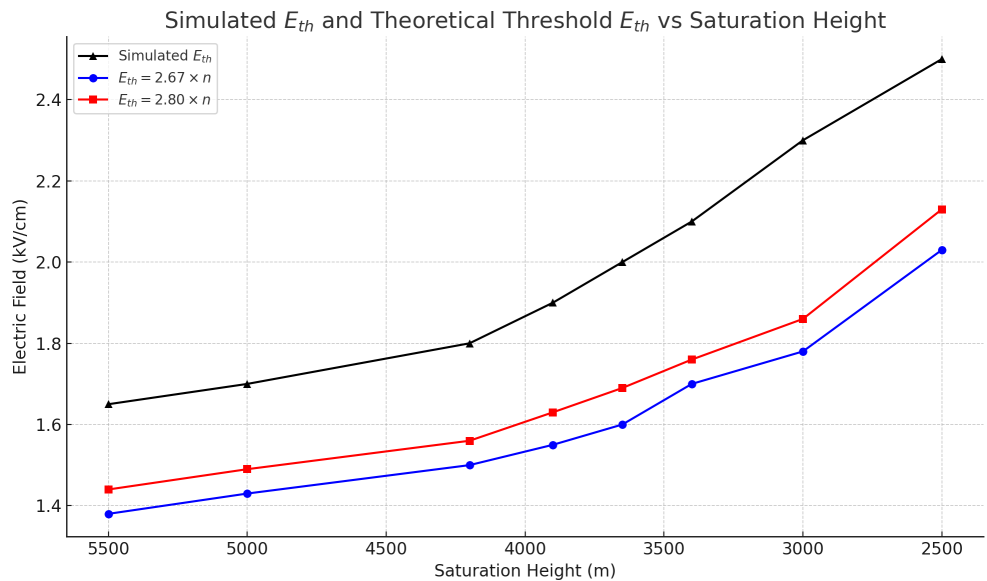144 avalanche particles stops rising, as shown in Fig. 5.

Figure 5. The electric field strengths (Eth) at the point when the RREA particle flux began to decline for 4 stations located at altitudes ranging from 2000 to 4100 meters.

In Figure 6 and Table 1, we compare the "simulated" threshold Ez with the theoretical ones. Simulations show higher values than theoretical estimates, especially for high Eth values (low altitudes) at all four research stations. The relative air density n is calculated using an exponential atmospheric model. Threshold fields are computed as $2.67 \times n$ and $2.80 \times n$, representing the updated and theoretical thresholds, respectively. The percentage of enhancement indicates how much the applied field exceeds the theoretical thresholds. Strong AEFs, where the cascade did not attenuate, were not included in the table.

156

Figure 6. The dependence of the heights in the atmosphere and the corresponding threshold AEF to start RREA for theoretical and simulated values.

Table 1. Excess of E_z over E_{th}. Stopping altitudes and theoretical threshold field comparisons for heights 2500- 5550 m.

Input E_z (kV/cm)	Enhancement Stops at h(m)	n (relative density)	2.67 × n (kV/cm)	2.80 × n (kV/cm)	Rel. Excess. (%) (2.80)	Rel. Excess. (%) (2.67)	Site
1.55	5510	0.465	1.24	1.30	19.0	24.8	LHAASO (4400 m)
1.65	5110	0.492	1.31	1.38	19.8	25.7	LHAASO (4400 m)
1.8	4200.0	0.558	1.49	1.56	15.2	20.8	Aragats (3200 m)
1.9	3900.0	0.582	1.55	1.63	16.6	22.3	Aragats (3200 m)
1.9	3734	0.595	1.59	1.67	14.0	19.5	Lomnicky Štít (2630 m)
2.0	3334	0.629	1.68	1.76	13.5	19.0	Lomnicky Štít (2630 m)

2.1	2700.0	0.687	1.84	1.92	9.1	14.4	Nor Amberd (2000 m)
2.2	2500.0	0.707	1.89	1.98	11.2	16.6	Nor Amberd (2000 m)

163

2. Discussion and conclusion

165 Although both the classical threshold field (Eth ≈ 2.80 × n kV/cm) and its updated
166 version (Eth ≈ 2.67 × n kV/cm) are derived under idealized assumptions, the difference
167 between them results from refinements in modeling particle energy loss processes. The
168 earlier estimate of 2.80 × n was based on basic energy balance considerations using older
169 ionization loss models and assumed monoenergetic electrons. This threshold is slightly
170 above the breakeven field, where energy gain equals average energy loss. The updated
171 2.67 × n value, introduced by Dwyer and Rassoul (2024), incorporates more accurate
172 relativistic Boltzmann solutions, improved ionization and bremsstrahlung cross-sections,
173 and a probabilistic treatment of runaway thresholds across realistic energy spectra. While
174 both thresholds assume idealized, field-aligned electron motion in a uniform medium, the
175 updated value is physically more consistent. It predicts a slightly lower field strength
176 needed for initial runaway. However, CORSIKA simulations show that this refined
177 threshold is insufficient for sustained avalanche growth under real atmospheric conditions
178 due to scattering and finite path effects. Moreover, it deviates more from the simulated
179 value than the "classical" 30-year-old estimate.
180
181 Multiple physical processes act to inhibit ideal runaway propagation. Coulomb scattering
182 with atmospheric nuclei and Møller scattering with electrons cause substantial angular
183 deflection and energy redistribution. Secondary electrons are not generated strictly along
184 the field direction, and many lose energy before gaining sufficient momentum to continue
185 avalanche growth. As a result, electrons must be accelerated in stronger-than-threshold
186 fields to overcome these losses and maintain avalanche conditions.
187 CORSIKA simulations, which incorporate all major interaction mechanisms—including
188 Coulomb and Møller scattering, bremsstrahlung losses, finite propagation distances, and
189 realistic secondary cosmic ray spectra—demonstrate that avalanches only fully develop
190 when the applied field exceeds the theoretical threshold by a measurable margin. For the
191 updated 2.67 × n value, we observe a required excess of approximately 20-22% at the
192 Aragats station (∼3200–4200 m a.s.l.), whereas for the classical 2.80 × n threshold, the
193 excess is typically 15-17%.
194 Interestingly, this required excess decreases with increasing air density, as observed in
195 the Nor Amberd simulations. At lower altitudes (∼2500–2700 m a.s.l.), the difference
196 between the applied and threshold fields is reduced: only 14–16% above 2.67 × n, and
197 about 9–11% above 2.80 × n. This trend can be explained as follows:
198 In denser air, the chances of energy loss interactions increase, but so does the likelihood
199 of electron multiplication through ionization and bremsstrahlung over shorter distances.
200 The avalanche can develop more quickly because seed electrons encounter more target

201 atoms in a given path length. As a result, the necessary "headroom" above the threshold
202 field for sustained multiplication is smaller. Simply put, the efficiency of avalanche
203 formation improves in denser air, even though the absolute threshold field is higher. This
204 results in a smaller relative excess being required above the theoretical threshold.
205
206 Therefore, although the threshold field scales linearly with air density, the required
207 enhancement factor does not. It decreases with increasing density due to a balance
208 between energy loss and multiplication processes, all of which are faithfully captured in
209 the CORSIKA simulation framework. This emphasizes the importance of altitude-
210 dependent analysis in interpreting Thunderstorm Ground Enhancements (TGEs) and
211 suggests that scaling laws based solely on density may overlook subtler effects arising
212 from atmospheric structure and shower development dynamics.
213
214 **Code and data availability**
215
216 Data archive on TGE event is reposted on the Mendelay site at
217 https://doi.org/10.17632/8gtdbch59z (Chilingarian et al., 2024).
218 Data archive on CORSIKA simulations (RREA development in the atmosphere above 4
219 sites) is available at the link:
220 http://crd.yerphi.am/CORSIKA_Simulations
221
222
223 **Author contribution**
224 AC and MZ designed the simulation experiments with the CORSIKA code, and LH
225 performed the simulations. AC prepared the manuscript with contributions from all co-
226 authors
227
231
232
233
234 **References**
235

236 Alexeenko V.V, Khaerdin.ov N.S, Lidvansky A.S, et al. (2002). Transient variations of
237 secondary cosmic rays due to atmospheric AEF and evidence for pre-lightning particle
238 acceleration. Phys Lett A 301:299–306.
239
240 Ambrozová I., Kákona M., Dvorák R., et al. (2023) Latitudinal effect on the position of
241 Regener–Pfotzer maximum investigated by balloon flight HEMERA 2019 in Sweden and
242 balloon flights FIK in Czechia, Radiation Protection Dosimetry 199(15–16), 2041.
243 doi.org/10.1093/rpd/ncac299
244

245   Babich, L. P., Donskoy, E. N., Kutsyk, I. M., & Kudryavtsev, A. Y. (2001). Comparison
246   of relativistic runaway electron avalanche rates obtained from Monte Carlo simulations
247   and kinetic equation solution. IEEE Transactions on Plasma Science, 29(3), 430-438.
248
249   S. Buitink, H. Falcke, et al. Monte Carlo simulations of air showers in atmospheric AEFs,
250   Astropart. Phys. 33 (2010) 1.
251
252   Chilingarian A., Mailyan B., and Vanyan L., Recovering the energy spectra of electrons
253   and gamma rays coming from the thunderclouds, Atmos. Res. 114–115, 1 (2012).
254
255   Chilingarian A., Hovsepyan G., Karapetyan T., et al. (2022), Development of the
256   relativistic runaway avalanches in the lower atmosphere above mountain altitudes, EPL,
257   139, 50001, https://doi.org/10.1209/0295-5075/ac8763
258
259   Chilingarian A., Karapetyan T. Aslanyan D., Sargsyan., B. (2024), Extreme thunderstorm
260   ground enhancements registered on Aragats in 2023", Mendeley Data, V1.
261   DOI:10.17632/8gtdbch59z. DOI: 10.17632/8gtdbch59z.6
262
263   Dwyer J.R. (2003) A fundamental limit on AEFs in air, Geophys. Res. Lett. 30, 2055.
264   doi.org/10.1029/2003GL017781
265
266   Dwyer G.R., Rassoul H.K. (2024) High energetic radiation from thunderstorms and
267   lightning, in Lightning Electromagnetics, IET series Volume 1, 365.
268
269   Gurevich, G., Milikh, R., Roussel-Dupre (1992) Runaway electron mechanism of air
270   breakdown and preconditioning during a thunderstorm, Physics Letters A 165 (5), 463.
271
272   Heck D., Knapp J., Capdevielle J. N., Schatz G., and Thouw T., Report No. FZKA 6019,
273   1998, Forschungszentrum, Karlsruhe, https://www.ikp.kit.edu/corsika/70.php.
274   Marshall, T. C., M. P. McCarthy, and W. D. Rust (1995), AEF magnitudes and lightning
275   initiation in thunderstorms, J. Geophys. Res., 100, 7097.

276   Sato, T. Analytical model for estimating the zenith angle dependence of terrestrial cosmic
277   ray fluxes. PLoS ONE 2016, 11, e0160390.

278   M. Stolzenburg, T. C. Marshall, W. D. Rust, E. Bruning, D. R. MacGorman, and T.
279   Hamlin (2007), AEF values observed near lightning flash initiations, Geophys. Res. Lett.,
280   34, L04804.

281   Symbalisty, E. M. D., R. A. Roussel-Dupré, and V. A. Yukhimuk (1998), Finite volume

282   solution of the relativistic Boltzmann equation for electron avalanche studies, IEEE

283   Trans. Plasma Sci., 26, 1575–1582.

284

285